

Terrain-Aware Rollover Prediction for Ground Vehicles Using the Zero-Moment Point Method

Sittikorn Lapapong and Sean N. Brennan*, *Member, IEEE*

Abstract—Rollover accidents are one of the leading causes of death in highway accidents due to their very high fatality rate. A key challenge in preventing rollover via chassis control is that the prediction of the onset of rollover can be quite difficult, especially in the presence of terrain features typical of roadway environments. These road features include superelevation of the road (e.g road bank), the median slope, and the shoulder down-slope. This work develops a vehicle rollover prediction algorithm that is based on a kinematic analysis of vehicle motion, a method that allows explicit inclusion of terrain effects. The solution approach utilizes the concept of zero-moment point (ZMP) that is typically applied to walking robot dynamics. This concept is introduced in terms of a lower-order model of vehicle roll dynamics to measure the vehicle rollover propensity, and the resulting ZMP prediction allows a direct measure of a vehicle rollover threat index. Simulation results using a complex multi-body vehicle simulation show the effectiveness of the proposed algorithm during different road geometry scenarios and driver excitations.

I. INTRODUCTION

According to the U.S. Department of Health and Human Services [1], motor vehicle accidents are the leading cause of death in the United State when causes of death by disease are not included. In 2007, automobile crashes claimed 41,059 lives, and 2,491,000 people were injured in 6,024,000 police-reported motor vehicle traffic crashes [2]. These reports indicate that 8,940 out of 41,059 lives were lost in rollover accidents, indicating that vehicle rollover is one of the major causes of death for highway accidents. To reduce deaths due to the vehicle rollover accidents, it is very important to improve vehicle safety, especially roll stability of the vehicle.

The first recorded automobile rollover tests were conducted at a GM testing facility in 1934 [3]. At that time, the tests primarily focused on structural integrity of vehicles. Research since this time has increasingly focused on measuring and predicting vehicle rollover propensity to produce rollover threat metrics that are useful for predicting rollover onset, thus providing a measurement for indicating a rollover-prone vehicle, for alerting the driver during a rollover-prone situation, or even for active chassis control to prevent rollover. These metrics can be generally categorized as follows: static or steady-state rollover metrics, dynamic rollover metrics, energy-based rollover metrics, rollover metrics based on thresholds of vehicle states or combinations of the vehicle states, and rollover metrics based on forces acting on tires or body moments generated by those forces.

Examples of static or steady-state rollover metrics include the Static Stability Factor (SSF) [4], [5], the Side-Pull Ratio (SPR) [4], [5], the Tilt-Table Ratio (TTR) [4], [5], the centrifuge test [5], the Bickerstaff's rollover index [6], and related rollover thresholds for a suspended vehicle model [7]. These metrics codify rollover propensity as a ratio between a force that attempts to roll a vehicle over and a force that attempts to recover the vehicle. All metrics except the SSF, the Bickerstaff's rollover index, and the rollover threshold for a suspended vehicle model are obtained from experiments. The dynamic rollover metrics are based on the Newton's second law of motion, and these include, for instance, the Dynamic Stability Index (DSI) [7]. Examples of energy-based metrics include the Critical Sliding Velocity (CSV) [8], [9], [10], [5], which is a minimum lateral velocity required to tip a vehicle over when the vehicle is sliding laterally and hitting a curb, and the Rollover Prevention Energy Reserve (RPER) [7], which is defined as the difference between the potential energy required to bring a vehicle to its tip-over position and the sum of the instantaneous linear and rotational kinetic energy.

One issue with the previous metrics is that they do not provide a situation-dependent warning. This issue can be addressed by using the vehicle states at a particular driving situation to anticipate rollover events. Examples of rollover metrics using vehicle states include Wielenga [11], Carlson and Gerdes [12], and Yoon *et al.* [13]. These studies use roll angle, roll rate, lateral acceleration, etc. or combinations thereof as a performance index to design rollover prevention control schemes. Similarly, rollover metrics can be based on situation-dependent tire forces and/or moments. Examples include the Load Transfer Ratio (LTR) [14] and the Stability Moment (SM) [15], which each are based on the forces acting on a vehicle's tires. An example using moments would be the study by Cameron [16] who predicted a minimum steering angle that caused vehicle rollover by determining the existence of a slide-before-roll condition. Finally, one can extend the prediction of vehicle states, forces, or moments into the future to anticipate rollover events. Examples include Chen and Peng who proposed Time-To-Rollover (TTR) [17].

For a rollover metric to be useful, the prediction of rollover behavior needs to be accurate, particularly the onset of rollover such as tire lift. Since, referring to a National Highway Traffic Safety Administration (NHTSA)'s report [18], the majority of all rollover accidents are due to either on-road tripped rollover or off-road rollover in which terrain plays a significant role, this research differentiates from previous studies to develop a more accurate tire-lift prediction

* Corresponding author

S. Lapapong and S. Brennan are with the Department of Mechanical and Nuclear Engineering, The Pennsylvania State University, University Park, PA 16802 USA sul174@psu.edu; sbrennan@psu.edu

by including the effects of terrain. There are quite a few rollover metrics (load transfer ratio and stability moment) that concern the influences of the terrain; however, the implementation of those metrics is still an issue. Additionally, once wheel liftoff occurs, the numerical values of these metrics artificially saturate (be either -1 or 1). Under this circumstance, the metrics are deprived of the sense of the severity of the encountering rollover situation. To deal with these matters, we adapt a method used by walking robots called the Zero-Moment Point (ZMP), a concept introduced in Section II of the paper. Section III discusses an application of the ZMP as a vehicle rollover threat index. The necessity of the terrain knowledge is presented in Section IV followed by simulation results in Section V to show fidelity of the proposed algorithm. Conclusions then summarize the main contributions of this paper.

II. ZERO-MOMENT POINT (ZMP)

The concept of zero-moment point (ZMP) was developed and introduced by Vukobratovic in 1968 [19], [20], [21]. This concept has been very useful and widely used in bipedal robotics research. Biped robotics scientists have applied the concept to preserve robots' dynamic balance during walking, or, in other words, to maintain stability of the robots, preventing the robots from overturning. There are hundreds of biped walking robots implemented with this algorithm, for instance, Honda's humanoid robots [22]. Moreover, many researchers used the ZMP as a stability constraint for mobile manipulators to prevent the overturn of the mobile manipulators due to their own dynamics [23], [24], [25], [26].

By definition, the zero-moment point is the point on the ground where the tipping moment acting on the biped, due to gravity and inertia forces, equals zero. Here, the tipping moments are defined as the component of the moment that is tangential to the supporting surface [27]. To be more strict, this zero-moment point must be within the support polygon of the mechanisms; otherwise, this point does not physically exist. If the location of the ZMP is calculated, and it is outside the support polygon, that point is considered as a fictitious ZMP (FZMP) [21]. To be more precise, it should be noted that the term ZMP is not a perfectly exact expression, because the normal component of the moment generated by the inertia forces acting on the biped is not necessarily zero. However, we should keep in mind that the term ZMP abridges the exact expression "zero tipping moment point" [27].

Considering a kinematic chain in Fig. 1 and using general equations of motion [28], [29], [26] and D'Alembert's principle [10], the moment equation about point A in Fig. 1 induced by inertial forces and gravity is:

$$M_A = \vec{p}_1 \times m_1 \vec{a}_{G_1} + \mathbf{I}_1 \dot{\vec{\omega}}_1 + \vec{\omega}_1 \times \mathbf{I}_1 \vec{\omega}_1 - \vec{p}_1 \times m_1 \vec{g} + \vec{p}_2 \times m_2 \vec{a}_{G_2} + \mathbf{I}_2 \dot{\vec{\omega}}_2 + \vec{\omega}_2 \times \mathbf{I}_2 \vec{\omega}_2 - \vec{p}_2 \times m_2 \vec{g} \quad (1)$$

where m_i is the mass of the i^{th} body, \mathbf{I}_i is the inertia tensor of the i^{th} body, \vec{a}_i is the linear acceleration of the i^{th} body, $\vec{\omega}_i$ is the angular velocity of the i^{th} body, $\vec{p}_i = \vec{r}_i - \vec{r}_{zmp}$,

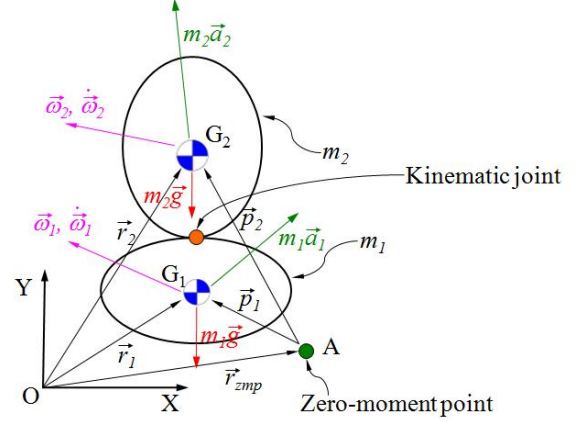


Fig. 1. Two-link kinematic chain

\vec{r}_i is the position vector of the center of gravity (CG) of the i^{th} body, \vec{r}_{zmp} is the position vector of the ZMP, and \vec{g} is gravitational acceleration. If $\vec{M}_A = [0 \ 0 \ M_{A_z}]^T$, the point A becomes a zero-moment point.

III. APPLICATION OF ZERO-MOMENT POINT AS VEHICLE ROLLOVER THREAT INDEX

In this section, the concept of the ZMP is applied as an indicator to predict vehicle rollover. A vehicle is modeled as a rigid vehicle model in Section III-A and as a vehicle roll model in Section III-B. The convention of the coordinates [30] and the sequence of coordinate rotations [31] used in this section are defined by the Society of Automotive Engineering (SAE).

A. Application to Rigid Vehicle Model

In this section, the concept of the ZMP is applied to a vehicle modeled as a rigid body shown in Fig. 2. The

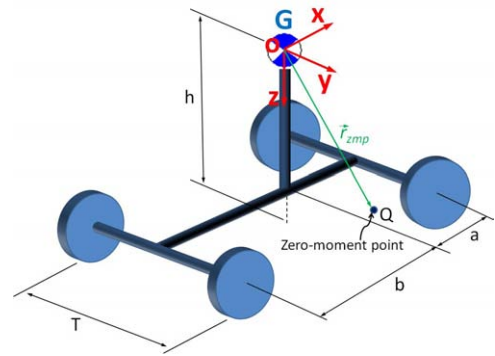


Fig. 2. Rigid vehicle model

nomenclature used in derivations of this section is defined in Table I, Fig. 2, and Fig. 3. In Fig. 2, the coordinates $oxyz$ are fixed with the vehicle at the center of gravity of the vehicle (point G). Point Q is a zero-moment point located by \vec{r}_{zmp} and is always physically on the ground.

To calculate the location of the zero-moment point, we assume that the vehicle is symmetrical in the xz -plane ($I_{xy} =$

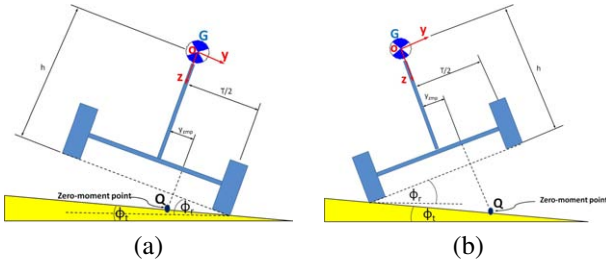


Fig. 3. Rigid vehicle model on terrain. (a) $\phi_r \ge \phi_t$ (b) $\phi_r < \phi_t$

TABLE I
NOMENCLATURE USED IN SECTION III-A

Symbol	Definition	Symbol	Definition
m	mass of vehicle	a	distance from CG to front axle
b	distance from CG to rear axle	h	height of CG
T	track width	$I_{xx,yy,zz}$	x-axis, y-axis, and z-axis mass moment of inertia
$I_{xz,yz}$	product mass moment of inertia	ϕ_r	roll angle of rigid vehicle model
ϕ_r	roll angle of rigid vehicle model	ϕ_t	roll angle of terrain
θ	pitch angle	ψ	yaw angle
p	roll rate	q	pitch rate
r	yaw rate		
a_G	CG's acceleration of rigid vehicle model ^a		

^a Subscripts x , y , and z indicate accelerations in x -, y -, and z -directions.

0), and the vehicle is free to move in any directions. Considering Fig. 3, the location of the ZMP may be expressed as:

$$\vec{r}_{zmp} = x_{zmp}\vec{i} + y_{zmp}\vec{j} + \left[h + \frac{T}{2} |\tan(\phi_r - \phi_t)| - y_{zmp} \tan(\phi_r - \phi_t) \right] \vec{k} \quad (2)$$

By using (1), the location of the ZMP can be expressed as:

$$x_{zmp} = \left\{ \frac{1}{2m[-g \cos(\theta) \cos(\phi_r) + a_{Gz}]} \right\} \left\{ -2I_{xx}p^2 - 2I_{yz}pq - 2I_{yy}\dot{q} - 2(I_{xx} - I_{zz})pr + 2I_{xz}r^2 + 2I_{yz}\dot{r} + 2mgh \sin(\theta) + mgT |\tan(\phi_r - \phi_t)| \sin(\theta) + 2mha_{Gx} + mTa_{Gx} |\tan(\phi_r - \phi_t)| + [(g \sin(\theta) + a_{Gx})(mT |\tan(\phi_r - \phi_t)| (-g \cos(\theta) \sin(\phi_r) + a_{Gy})) + 2(I_{xx}p - I_{xz}pq - I_{yz}q^2 - (I_{yy} - I_{zz})qr + I_{yz}r^2 - I_{xz}\dot{r} - mgh \cos(\theta) \sin(\phi_r) + mha_{Gy})) \tan(\phi_r - \phi_t)] / [g \cos(\theta) \cos(\phi_t) \sec(\phi_r - \phi_t) - a_{Gz} - a_{Gy} \tan(\phi_r - \phi_t)] \right\} \quad (3)$$

$$y_{zmp} = \left\{ mT |\tan(\phi_r - \phi_t)| [g \cos(\theta) \sin(\phi_r) - a_{Gy}] + 2[-I_{xx}\dot{p} + I_{xz}pq + I_{yz}q^2 + (I_{yy} - I_{zz})qr - I_{yz}r^2 + I_{xz}\dot{r} + mgh \cos(\theta) \sin(\phi_r) - mha_{Gy}] / \{ 2m [g \cos(\theta) \cos(\phi_t) \sec(\phi_r - \phi_t) - a_{Gz} - a_{Gy} \tan(\phi_r - \phi_t)] \} \right\} \quad (4)$$

B. Application to Vehicle Roll Model

A vehicle is modeled as illustrated in Fig. 4. The vehicle consists of two parts: unsprung mass and sprung mass. Both masses are linked together at the point called a roll center (point R). The roll center allows the sprung mass to rotate only in the roll direction (about the x -axis), allowing the unsprung mass and sprung mass have the same angular velocities and accelerations except in the roll direction. The sprung mass is supported by a roll spring (K_ϕ) and roll damper (D_ϕ) that act as the vehicle's suspensions. In the figure, point G

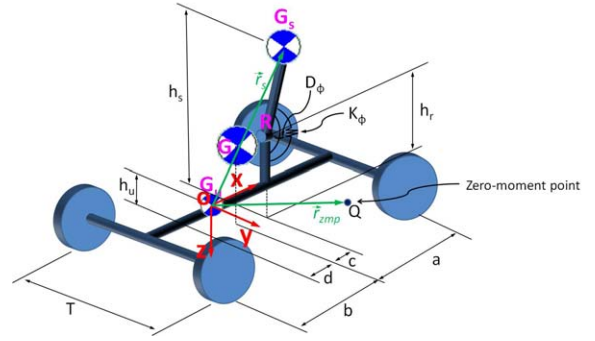


Fig. 4. Vehicle roll model

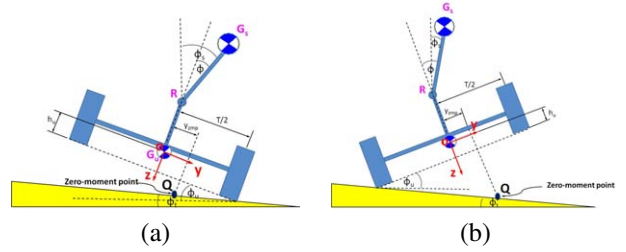


Fig. 5. Vehicle roll model on terrain. (a) $\phi_u \ge \phi_t$ (b) $\phi_u < \phi_t$

is the location of the whole vehicle's center of gravity (CG). Point G_u and point G_s are the centers of gravity of unsprung mass's and sprung mass's, respectively. The sprung mass's CG is located by \vec{r}_s , which is $(c + d)\vec{i} + (h_s - h_r) \sin(\phi)\vec{j} + [h_u + h_r(\cos(\phi) - 1) - h_s \cos(\phi)]\vec{k}$. The notations used in this section are defined in Table II, Fig. 4, and Fig. 5. The coordinates $oxyz$ are attached with the unsprung mass's center of gravity whose distance is d measured from the vehicle's CG. Point Q in Fig. 4 is the zero-moment point, which is located by \vec{r}_{zmp} .

In the same fashion as in Section III-A, the position vector of the ZMP may be expressed as:

$$\vec{r}_{zmp} = x_{zmp}\vec{i} + y_{zmp}\vec{j} + \left[h_u + \frac{T}{2} |\tan(\phi_u - \phi_t)| + y_{zmp} \tan(\phi_u - \phi_t) \right] \vec{k} \quad (5)$$

The location of the ZMP can be solved by using (1), which is:

$$x_{zmp} = \left\{ -2(I_{yy}s + I_{yy}u)\dot{q} + 2(I_{xz}s + I_{xz}u)r^2 + 2(I_{yz}s + I_{yz}u)\dot{r} - 2m_s g(c + d) \cos(\theta) \cos(\phi_u) + m_s(g \sin(\theta) + a_{sx})T |\tan(\phi_t - \phi_u)| + 2m_s a_{sz}(c + d) + 4m_s(g \sin(\theta) + a_{sx})h_r \sin^2\left(\frac{\phi}{2}\right) + 2m_s(g \sin(\theta) + a_{sx})h_s \cos(\phi) + m_u(g \sin(\theta) + a_{ux})T |\tan(\phi_t - \phi_u)| + 2m_u(g \sin(\theta) + a_{ux})h_u - 2I_{yz}s p_s q - 2(I_{xx}s - I_{zz}s)p_s r - 2I_{xz}s p_s^2 - 2I_{yz}u p_u q - 2(I_{xx}u - I_{zz}u)p_u r - 2I_{xz}u p_u^2 + [(m_s(g \sin(\theta) + a_{sx}) + m_u(g \sin(\theta) + a_{ux})) (T |\tan(\phi_t - \phi_u)| (m_s(g \cos(\theta) \sin(\phi_u) - a_{sy}) + m_u(g \cos(\theta) \sin(\phi_u) - a_{uy})) + 2((I_{yz}s + I_{yz}u)q^2 + (I_{yy}s + I_{yy}u - I_{zz}u)qr - (I_{yz}s + I_{yz}u)r^2 + (I_{xz}s + I_{xz}u)r + m_s h_r(-2g \cos(\theta) \cos\left(\frac{\phi}{2} + \phi_u)\right) \sin\left(\frac{\phi}{2}\right) - 2a_{sy} \sin^2\left(\frac{\phi}{2}\right) + a_{sz} \sin(\phi)) + m_s h_s(g \cos(\theta) \sin(\phi + \phi_u) - a_{sy} \cos(\phi) - a_{sz} \sin(\phi)) + m_u g h_u \cos(\theta) \sin(\phi_u) - m_u a_{uy} h_u + I_{xz}s p_s q + I_{xz}u p_u q - I_{xx}s \dot{p}_s - I_{xx}u \dot{p}_u) \tan(\phi_t - \phi_u) / [m_s(g \cos(\theta) \cos(\phi_t) \sec(\phi_t - \phi_u) - a_{sz} + a_{sy} \tan(\phi_t - \phi_u)) + m_u(g \cos(\theta) \cos(\phi_t) \sec(\phi_t - \phi_u) - a_{uz} + a_{uy} \tan(\phi_t - \phi_u))] \right\} / \{ 2m_s [-g \cos(\theta) \cos(\phi_u) + a_{sz}] + 2m_u [-g \cos(\theta) \cos(\phi_u) + a_{uz}] \} \quad (6)$$

TABLE II
NOMENCLATURE USED IN SECTION III-B

Symbol	Definition	Symbol	Definition
m	mass of vehicle ^a	a	distance from vehicle CG to front axle
b	distance from vehicle CG to rear axle	c	distance from vehicle CG to sprung mass's CG
d	distance from vehicle CG to unsprung mass's CG	h_u	height of unsprung mass's CG
h_s	height of sprung mass's CG	h_r	height of roll center
T	track width	$I_{x,x,y,y,z,z}$	x-axis, y-axis, and z-axis mass ^a moment of inertia
$I_{x,z,y,z}$	product mass moment of inertia ^a	ϕ_u	roll angle of unsprung mass
ϕ_u	roll angle of unsprung mass	ϕ_s	roll angle of sprung mass
ϕ	$\phi_s - \phi_u$	ϕ_t	roll angle of terrain
θ	pitch angle	p	roll rate ^a
ψ	yaw angle	r	yaw rate
q	pitch rate	a_u	acceleration of unsprung mass's CG ^b
a_u	acceleration of unsprung mass's CG ^b	a_s	acceleration of sprung mass's CG ^b

^a Subscripts u and s indicate the properties of unsprung mass and sprung mass of the vehicle roll model, respectively.

^b Subscripts x , y , and z indicate accelerations in x -, y -, and z - directions.

$$\begin{aligned}
y_{zmp} = & \{T |\tan(\phi_t - \phi_u)| [m_s(-g \cos(\theta) \sin(\phi_u) + a_{sy}) + m_u(-g \cos(\theta) \\
& \sin(\phi_u) + a_{uy})] - 2 [(I_{yzs} + I_{yzu})q^2 + (I_{yys} + I_{yyu} - I_{zzs} - I_{zzu})qr \\
& - (I_{yzs} + I_{yzu})r^2 + (I_{xzs} + I_{xzu})\dot{r} + m_s h_r(-2g \cos(\theta)) \cos\left(\frac{\phi}{2} + \phi_u\right) \\
& \sin\left(\frac{\phi}{2}\right) - 2a_{sy} \sin^2\left(\frac{\phi}{2}\right) + a_{sz} \sin(\phi)] + m_s h_s (g \cos(\theta) \sin(\phi + \phi_u) \\
& - a_{sy} \cos(\phi) - a_{sz} \sin(\phi)] + m_u h_u (g \cos(\theta) \sin(\phi_u) - m_u h_u a_{uy} + I_{xzs} p s q \\
& + I_{xzu} p u q - I_{xzs} \dot{p} s - I_{xzu} \dot{p} u)\} / \{2 [m_s (g \cos(\theta) \cos(\phi_t) \sec(\phi_t - \phi_u) \\
& - a_{sz} + a_{sy} \tan(\phi_t - \phi_u)] + m_u (g \cos(\theta) \cos(\phi_t) \sec(\phi_t - \phi_u) - a_{uz} \\
& + a_{uy} \tan(\phi_t - \phi_u)]\} \quad (7)
\end{aligned}$$

IV. TERRAIN INFORMATION

From Section III, one can see that the knowledge of terrain profile is critical, especially a slope of a road (ϕ_t). Currently, there are many ways to obtain terrain information. One practical way is to use a light-detection-and-ranging (LIDAR) scanning system [32]. In this system, a LIDAR-equipped vehicle scans a road at a particular yaw angle and constructs a terrain database. The terrain database basically contains a roll angle ϕ_d and pitch angle θ_d of the terrain as well as a yaw angle ψ_d of the scanning vehicle. However, for the proposed rollover prediction algorithms described in Section III, a yaw angle of a vehicle implementing the algorithms is not always the same as the one in the terrain database. Therefore, some kind of transformation is needed. Considering Fig. 6 to figure out a roll angle of terrain at any particular yaw angle, we can write:

$$\sin(\phi_t) = \cos(\nu) = \frac{\vec{r}_E \cdot \vec{n}}{|\vec{r}_E| |\vec{n}|} \quad (8)$$

where ϕ_t is the roll angle of terrain at any particular yaw angle, ν is an angle between \vec{n} and a horizontal plane, \vec{n} is a vertical unit vector, which is $\vec{n} = -\sin(\theta_d)\vec{i} + \sin(\phi_d)\cos(\theta_d)\vec{j} + \cos(\phi_d)\cos(\theta_d)\vec{k}$, and \vec{r}_E is a vector that represents a location of point E in Fig. 6. The vector \vec{r}_E ,

which can be written as a function of that instant yaw angle and the yaw angle of the scanning vehicle that is stored in the terrain database, ψ_d , is $[-T \sin(\psi - \psi_d)]\vec{i} + [T \cos(\psi - \psi_d)]\vec{j}$. By substituting all defined vectors in (8), the roll angle of terrain at any particular yaw angle may be expressed as:

$$\phi_t = \arcsin [\sin(\psi - \psi_d) \sin(\theta_d) + \sin(\phi_d) \cos(\theta_d) \cos(\psi - \psi_d)] \quad (9)$$

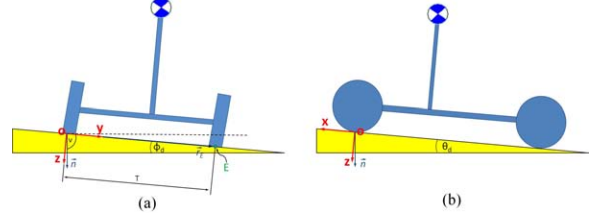


Fig. 6. Vehicle running on a slope. (a) Rear-viewed. (a) Side-viewed.

V. RESULTS

In this section, the proposed rollover prediction algorithms from both the rigid vehicle model (4) and the vehicle roll model (7) are implemented. CarSim, which is a vehicle simulation software, was used to simulate a real vehicle. Vehicle parameters used in simulations were taken from [33], [17]. The parameters were modified and summarized in Table III. The algorithms were tested in two different scenarios, which are a flat road and banked road. In each scenario, the vehicle was excited in the way such that wheel liftoff and rollover were induced. A Toyota's J-turn and double lane change are two primary maneuvers used throughout the simulations. Under the Toyota's J-turn maneuver, the vehicle was first steered to the left and then the right. To determine when wheel liftoff has occurred, the Load Transfer Ratio (LTR) [14] was used as an indicator. The LTR is defined as:

$$LTR = \frac{F_{z_R} - F_{z_L}}{F_{z_R} + F_{z_L}} \quad (10)$$

where F_{z_L} and F_{z_R} are normal forces acting on tires on left and right sides of the vehicle, respectively. The LTR ranges from -1 to 1, and once the wheel liftoff occurs, the absolute value of the LTR is equal to one.

A. Results on Flat Road

The LTRs and displacements of y_{zmp} calculated from (4) and (7) of the vehicle that was excited by a Toyota's J-turn on a flat road, leading to the wheel liftoff and rollover, are plotted in Figs. 7 and 8, respectively. Fig. 9 are the results during the double lane change maneuvers on the flat road that induced the wheel liftoff, and the results of the rollover case are in Fig. 10. The shaded regions in the figures indicate the regions where wheel liftoff has occurred in the CarSim simulations.

TABLE III
VEHICLE PARAMETERS

Symbol	Value	Unit	Symbol	Value	Unit
m	1843	kg	m_u	180	kg
m_s	1663	kg	a	1.175	m
b	1.403	m	c	0.028	m
d	0.257	m	T	1.565	m
h	0.847	m	h_u	0.36	m
h_s	0.9	m	h_r	0.494	m
I_{xx}	762.09	kg·m ²	I_{yy}	2857.56	kg·m ²
I_{zz}	3074.32	kg·m ²	I_{xz}	59.98	kg·m ²
I_{yz}	0	kg·m ²	I_{xu}	61.73	kg·m ²
I_{yu}	346.37	kg·m ²	I_{zu}	357.13	kg·m ²
I_{xu}	0	kg·m ²	I_{zu}	0	kg·m ²
I_{xs}	653	kg·m ²	I_{ys}	2498	kg·m ²
I_{zs}	2704	kg·m ²	I_{xs}	85	kg·m ²
I_{ys}	0	kg·m ²	g	9.81	m/s ²

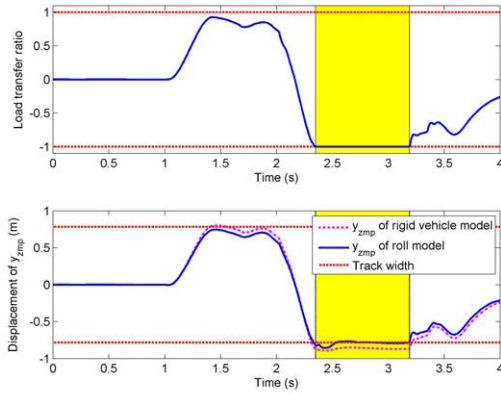


Fig. 7. LTR and displacements of y_{zmp} of vehicle during Toyota's J-turn on flat road, causing wheel liftoff.

B. Results on Banked Road

A banked road constructed in simulations is a 30%-graded road (16.70 degrees of an inclination angle). Figs. 11 and 12 illustrate the LTRs and displacements of y_{zmp} of the vehicle getting wheel liftoff and rolling over, respectively, during the Toyota's J-turn. The results of the vehicle from the double lane change maneuver that caused wheel liftoff are shown in Fig. 13. Fig. 14 plots the LTR and displacement of y_{zmp} of the vehicle that rolled over under the double lane change excitation. The wheel liftoff regions in the figures are shaded.

C. Discussion on Results

A few observations can be seen from the results. First, the displacements of y_{zmp} from both the rigid vehicle model and the roll model predict vehicle rollover quite well; however, the displacement of y_{zmp} estimated from the rigid vehicle model (from (4)) is more conservative than the one obtained from the roll model (from (7)). This may happen since the roll model is more realistic than the rigid vehicle model, making the behaviors of the roll model closer to a real vehicle than those of the rigid vehicle model. The second observation is that the displacement of y_{zmp} during wheel liftoff is a

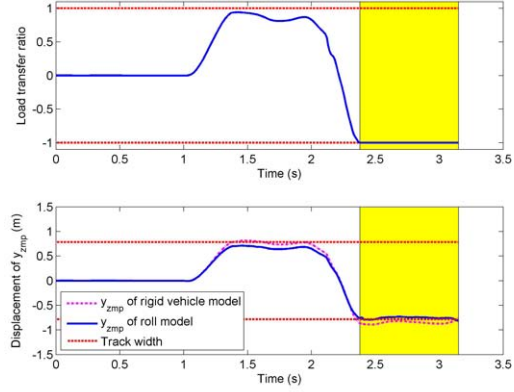


Fig. 8. LTR and displacements of y_{zmp} of vehicle during Toyota's J-turn on flat road, causing rollover.

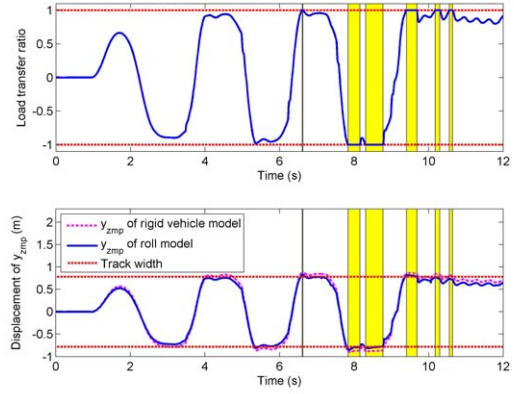


Fig. 9. LTR and displacements of y_{zmp} of vehicle during double lane change on flat road, causing wheel liftoff.

relatively flat straight line. Since there is no external force applied to the vehicle, the only place that reaction forces can physically act after the wheel liftoff is on the edge of the vehicle, allowing the vehicle to rock itself on its wheels due to the effects of its own momentum. Thus we see that the ZMP method also saturates as do other metrics, but this saturation is due to physics and not an artificial constraint. The last observation that one can notice is that the shapes of the LTRs and displacements of y_{zmp} are remarkably similar. The shape similarity comes from the fact that the zero-moment-point technique is an alternative way to represent load transfer, yet one that avoids any direct calculation of wheel normal forces.

Furthermore, Table IV shows the averages of the absolute values at wheel liftoff and average percent errors from y_{zmp} derived from the rigid vehicle model and vehicle roll model. These are compared against the Static Stability Factor (SSF) [4], [5], which is:

$$SSF = \frac{T}{2h} = \frac{aG_y}{g} \quad (11)$$

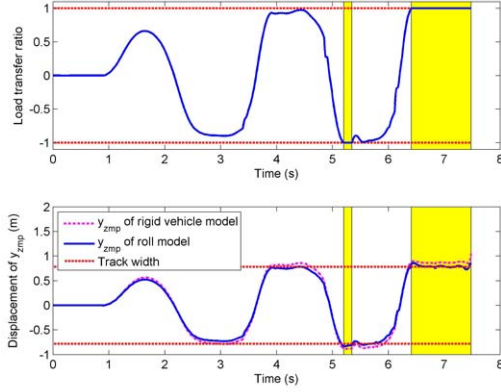


Fig. 10. LTR and displacements of y_{zmp} of vehicle during double lane change on flat road, causing rollover.

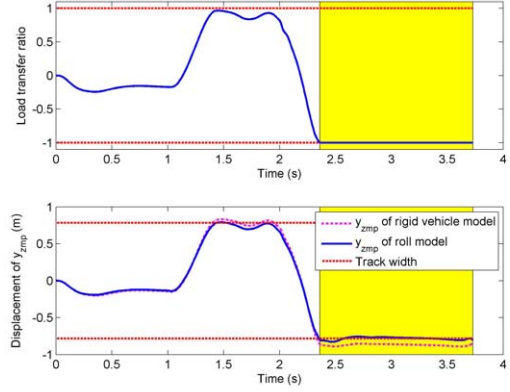


Fig. 12. LTR and displacements of y_{zmp} of vehicle during Toyota's J-turn on banked road, causing rollover.

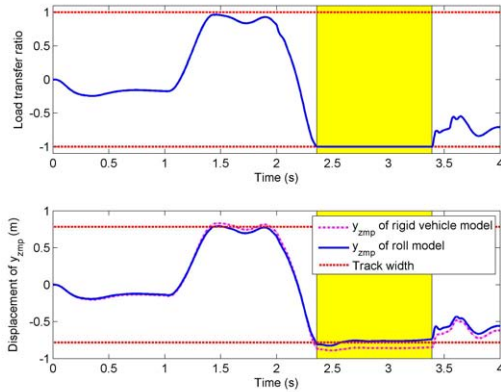


Fig. 11. LTR and displacements of y_{zmp} of vehicle during Toyota's J-turn on banked road, causing wheel liftoff.

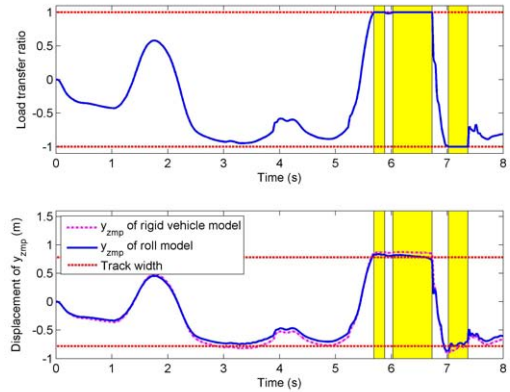


Fig. 13. LTR and displacements of y_{zmp} of vehicle during double lane change on banked road, causing wheel liftoff.

and Dynamic Stability Index (DSI) [7], which is:

$$DSI = \frac{T}{2h} = \frac{a_{Gy}}{g} - \frac{I_{xx}p}{mgh} \quad (12)$$

The nomenclature in (11) and (12) is defined in Table I. The reason behind using the average values is that, in some scenarios, wheel liftoff happens more than once. From Table IV, one can see that both SSF and DSI cannot predict wheel liftoff as precisely as the ZMP-based rollover indices proposed in this work, especially when the influence of terrain is present.

VI. CONCLUSIONS

The concept of the ZMP has been introduced and an application of the ZMP point as a rollover threat index for ground vehicles has been presented. From the simulation results, one can see that the ZMP is a valid indicator to measure the vehicle rollover propensity. Both rigid vehicle model and roll model predict the vehicle rollover well. Further, the roll model, as expected, predicts the vehicle rollover more precisely than the rigid vehicle model does due to more realistic assumptions of the roll model.

This work is still ongoing. Field experiments are being set up to confirm the effectiveness of the proposed algorithm, and a rollover mitigation control based on the ZMP will be designed to improve vehicle roll stability.

VII. ACKNOWLEDGEMENTS

Sittikorn Lapamong gratefully acknowledges the financial support from the Ministry of Science and Technology, the Royal Thai Government.

REFERENCES

- [1] M. Heron, D. L. Hoyert, S. L. Murphy, J. Xu, K. D. Kochanek, and B. Tejada-Vera, "Deaths: Final data for 2006," *National Vital Statistics Reports*, vol. 57, no. 14.
- [2] NHTSA's National Center for Statistics and Analysis, "Traffic safety facts: 2007 data," DOT HS 810 993.
- [3] R. A. Wilson and R. R. Gannon, "Rollover testing," *SAE Tech. Paper Series*, no. 720495, 1972.
- [4] J. P. Chrstos and D. A. Guenther, "The measurement of static rollover metrics," *SAE Tech. Paper Series*, no. 920582, 1992.
- [5] Transportation Research Board, *The National Highway Traffic and Safety Administration's Rating System for Rollover Resistance*. Washington, D.C.: National Academy Press, 2002.
- [6] D. J. Bickerstaff, "The handling properties of light trucks," *SAE Tech. Paper Series*, no. 760710, 1976.

TABLE IV

WHEEL-LIFT PREDICTIONS AND PERCENT ERRORS FROM Y_{ZMP} DERIVED FROM RIGID VEHICLE MODEL AND VEHICLE ROLL MODEL, STATIC STABILITY FACTOR (SSF) AND DYNAMIC STABILITY INDEX (DSI)

Condition and Maneuver	Static Stability Factor (SSF) Threshold = 0.924		Dynamic Stability Index (DSI) Threshold = 0.924		Y_{zmp} (rigid vehicle model) Threshold = 0.7825		Y_{zmp} (vehicle roll model) Threshold = 0.7825	
	Average of absolute value at wheel lift	Average percent error	Average of absolute value at wheel lift	Average percent error	Average of absolute value at wheel lift	Average percent error	Average of actual absolute value at wheel lift	Average percent error
FR ^a , TJ ^b , WL ^c	0.757	18.1	0.770	16.7	0.8775	12.1	0.8232	5.2
FR, TJ, RO ^d	0.806	12.8	0.843	8.8	0.8682	11.0	0.7560	3.4
FR, DLC ^e , WL	0.759	17.9	0.752	18.6	0.8607	10.0	0.8006	4.6
FR, DLC, RO	0.808	12.6	0.795	14.0	0.8778	12.2	0.8293	6.0
BR ^f , TJ, WL	0.473	48.8	0.473	48.8	0.8618	10.1	0.8049	2.9
BR, TJ, RO	0.473	48.8	0.473	48.8	0.8599	9.9	0.8034	2.7
BR, DLC, WL	0.967	9.6	0.967	9.6	0.8777	12.2	0.8350	6.7
BR, DLC, RO	0.784	27.6	0.785	27.5	0.8518	8.9	0.8120	3.8

^a FR = flat road, ^b TJ = Toyota's J-turn, ^c WL = wheel liftoff, ^d RO = rollover, ^e DLC = double lane change, ^f BR = banked road

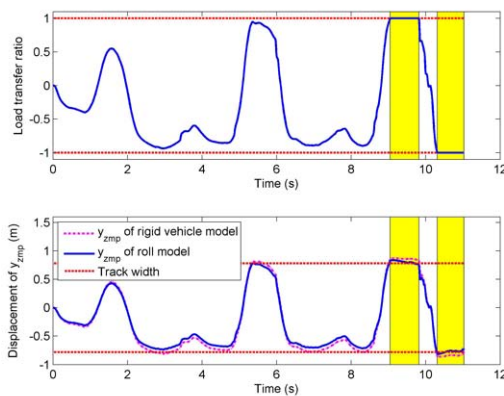


Fig. 14. LTR and displacements of y_{zmp} of vehicle during double lane change on banked road, causing rollover.

- [7] R. V. Dukkipati, J. Pang, M. S. Qatu, G. Sheng, and Z. Shuguang, *Road Vehicle Dynamics*. Warrendale, PA: Society of Automotive Engineers, Inc., 2008.
- [8] I. S. Jones, "Road accident studies with particular reference to the handling and stability characteristics of cars," Ph.D. dissertation, University College London, 1973.
- [9] Y. I. Lund and J. E. Bernard, "Analysis of simple rollover metrics," *SAE Tech. Paper Series*, no. 950306, 1995.
- [10] J. L. Meriam and L. G. Kraige, *Engineering Mechanics: Dynamics*, 4th ed. New York, NY: John Wiley & Sons, Inc., 1997.
- [11] T. J. Wielenga and M. A. Chace, "A study in rollover prevention using anti-rollover braking," *SAE Tech. Paper Series*, no. 2000-01-1642, 2000.
- [12] C. R. Carlson and J. C. Gerdes, "Optimal rollover prevention with steer by wire and differential braking," in *Proc. 2003 ASME IMECE*, vol. 72 DSC, no. 1, Washington, DC, Nov. 2003, pp. 345–354.
- [13] J. Yoon, D. Kim, and K. Yi, "Design of a rollover index-based vehicle stability control scheme," *Veh. Syst. Dyn.*, vol. 45, no. 5, pp. 459–475, 2007.
- [14] R. D. Ervin and Y. Guy, "The influence of weights and dimensions on the stability and control of heavy-duty trucks in Canada Volume I," The University of Michigan Transportation Institute, Ann Arbor, MI, Tech. Rep. UMTRI-86-35/I, July 1986.
- [15] S. C. Peters and K. Iagnemma, "Stability measurement of high-speed vehicles," *Veh. Syst. Dyn.*, vol. 47, no. 6, pp. 701–720, 2008.
- [16] J. T. Cameron, "Vehicle dynamic modeling for the prediction and prevention of vehicle rollover," Master's thesis, The Pennsylvania State University, 2005.
- [17] B.-C. Chen and H. Peng, "Differential-braking-based rollover preven-
- tion for sport utility vehicle with human-in-the-loop," *Veh. Syst. Dyn.*, vol. 36, no. 4-5, pp. 359–389, 2001.
- [18] National Highway Traffic Safety Administration, "An experimental examination of selected maneuvers that may induce on-road, untripped light vehicle rollover—phase I-A of NHTSA's 1997-1998 vehicle rollover research program," DOT HS 809 357.
- [19] M. Vukobratović and D. Juričić, "Contribution to the synthesis of biped gait," in *Proc. IFAC Symp. Technical and Biological Problem on Control*, Erevan, USSR, 1968.
- [20] M. Vukobratović, B. Borovic, D. Surla, and D. Stolić, *Biped Locomotion—Dynamics, Stability, Control, and Application*. Berlin, Germany: Springer-Verlag, 1990.
- [21] M. Vukobratović and B. Borovic, "Zero-moment point—thirty five years of its life," *Int. J. Humanoid Robotics*, vol. 1, no. 1, pp. 157–173, Mar. 2004.
- [22] K. Hirai, M. Hirose, Y. Haikawa, and T. Takenaka, "The development of honda humanoid robot," in *Proc. IEEE Int. Conf. on Robotics and Automation*, vol. 2, Leuven, Belgium, May 1998, pp. 1321–1326.
- [23] S. Sugano, Q. Huang, and I. Kato, "Stability criteria in controlling mobile robotic systems," in *Proc. IEEE Int. Conf. on Intelligent Robots and Systems*, Tokyo, Japan, July 1993, pp. 832–838.
- [24] Q. Huang and S. Sugano, "Manipulator motion planning for stabilizing a mobile-manipulator," in *Proc. IEEE Int. Conf. on Intelligent Robots and Systems*, vol. 3, Pittsburgh, PA, Aug. 1995, pp. 467–472.
- [25] S. Furuno, M. Yamamoto, and A. Mohri, "Trajectory planning of mobile manipulator with stability considerations," in *Proc. IEEE Int. Conf. on Robotics and Automation*, vol. 3, Taipei, Taiwan, Sept. 2003, pp. 3403–3408.
- [26] J. Kim and W. K. Chung, "Real-time zero moment point compensation method using null motion for mobile manipulators," *Advanced Robotics*, vol. 20, no. 5, pp. 581–593, 2006.
- [27] P. Sardain and G. Bessonnet, "Forces acting on a biped robot. center of pressure—zero moment point," *IEEE Trans. Syst., Man, Cybern. A*, vol. 34, no. 5, pp. 630–637, Sept. 2004.
- [28] H. Baruh, *Analytical Dynamics*. Singapore: McGraw-Hill Book Co., 1999.
- [29] A. Dasgupta and Y. Nakamura, "Making feasible walking motion of humanoid robots from human motion capture data," in *Proc. IEEE Int. Conf. on Robotics and Automation*, vol. 2, Detroit, MI, May 1999, pp. 1044–1049.
- [30] W. F. Milliken and D. L. Milliken, *Race Car Vehicle Dynamics*. Warrendale, PA: Society of Automotive Engineers, Inc., 1995.
- [31] "Vehicle dynamics terminology—SAE J670e," Society of Automotive Engineering, Inc., Warrendale, PA, Tech. Rep., Jul 1976.
- [32] P. K. Vemulapalli and S. N. Brennan, "Design and testing of a terrain mapping system for median slope measurement," in *Proc. 88th Annual Meeting of the Transportation Research Board*, Washington, D. C., Jan. 2009.
- [33] T. J. Wielenga, "Vehicle dynamics modeling for the national advanced driving simulator of a 1997 Jeep Cherokee," *SAE Tech. Paper Series*, no. 1999-01-0121, 1999.